Selected DNA Aptamers as Hydroxyapatite Affinity

Reagents

Emma Duffy, John Florek, Stephanie Colon, and Aren E. Gerdon*

Emmanuel College, Department of Chemistry and Physics, 400 The Fenway, Boston, MA 02115

*Corresponding Author: Aren E. Gerdon, gerdoar@emmanuel.edu, 617-735-9769

KEYWORDS: DNA, aptamer, hydroxyapatite, adsorption, labeling, microscopy

DNA aptamers were selected for their ability to bind specifically and quickly to crystalline

hydroxyapatite (Ca₁₀(PO₄)₆(OH)₂; HAP), the primary mineral component of enamel and bone.

Aptamers were found to have an enhanced percent of G-nucleotides and a propensity for forming

a G-quadruplex secondary structure. One aptamer was studied in comparison to control sequences

and was found to bind with high affinity and at high loading capacity, with enhanced binding

kinetics, and with specificity for crystalline HAP material over amorphous calcium phosphate

(ACP) and \(\beta\)-tricalcium phosphate (TCP). The fluorescently-functionalized aptamer was

demonstrated to specifically label HAP in a surface binding experiment and suggests the

usefulness of this selected aptamer in biomedical or biotechnology fields where the labeling of

specific calcium phosphate materials is required.

1

1. Introduction

DNA aptamers are short sequences of DNA that have been identified in a high throughput selection, such as SELEX (Systematic Evolution of Ligands by Exponential Enrichment).[1,2] Aptamers have been widely studied as affinity reagents and have been employed in countless biosensors to detect or label small molecules, proteins, cells, and other molecular targets, [2-11] but have not been fully explored in relation to heterogeneous interfaces or materials chemistry. Two notable exceptions of SELEX-identified aptamers for materials include the selection and deep sequencing to identify an aptamer with affinity for zinc oxide[12] and a Precipitation SELEX method to identify aptamers with an ability to promote mineralization of calcium phosphates.[13] Other research has explored the interface between nanomaterials and rationally-designed or existing polynucleotide sequences. This includes the silica mineralization of DNA origami, [14] gold nanoparticle-DNA interfaces,[15] recent work by the Liu group interfacing a range of materials with polynucleotides,[16-20] and others.[20,21] These examples have not taken advantage of the SELEX evolutionary procedure for identifying new sequences or motifs with material-binding properties, but do highlight the broad ability for polynucleotides to interface with materials. Through a SELEX or screening protocol new aptamers sequences may be identified that are able to act as affinity or labeling reagents for materials and biomaterials, thus expanding the applicability of DNA aptamers.

In this work, we present an affinity-based selection attempting to identify DNA aptamers with selectivity and enhanced kinetic binding to hydroxyapatite (Ca₁₀(PO₄)₆(OH)₂; HAP). HAP is an important biomaterial with medical implications in bone and enamel regeneration. A variety of molecules, proteins, polymers, and nanomaterials, both native and biomimetic, have been studied due to their interaction with calcium phosphate materials with the goal of understanding and

controlling the mineralization process.[22-27] We have pursued DNA aptamers due to the adaptability of the SELEX procedure, possibility for aptamer programmability, ease of synthesis, and natural structural connection to HAP through the DNA aptamer phosphate backbone. We have previously demonstrated the biomimetic role that DNA aptamers can play in the mineralization process[13,28,29] and complementary research has supported this, including computational studies[30,31] and work with DNA nanotubes[32]. We now present the role that aptamers play as affinity reagents or labeling reagents and envision that a selective and competitive HAP binder could be useful analytically in the labeling, in vitro or in vivo, of unknown calcium phosphate materials. Currently available labeling reagents typically actuate by fluorescing in the presence of soluble calcium cation, but do not bind to or label the biomaterial itself.[33] These reagents, therefore, are not able to distinguish between amorphous and crystalline material. This distinction can be extremely important, for example, in the analysis of transient amorphous mineral observed in early stages of enamel formation[34] or in identifying calcified arterial plaques.[35] The introduction of a material-specific DNA aptamer may prove to be useful in such cases and in the future analysis of mineralized materials or tissues.

2. Materials and Methods

2.1 Chemicals. Calcium chloride dihydrate (≥99.5%), dibasic sodium phosphate (≥99.0%), trizma hydrochloride (≥99.0%), glycine hydrochloride (≥99%), amorphous calcium phosphate (ACP, <100 nm), and hydroxyapatite nanopowder (HAP, <200 nm and ≥97% purity) were purchased from Sigma-Aldrich. Sodium chloride (≥99.5%), magnesium chloride hexahydrate (≥99%), and β-tri-calcium phosphate (TCP, ≥98%) were purchased from Fluka. Calcium hydroxyapatite standard was purchased from NIST. DNA aptamers were purchased from Integrated DNA Technologies and were reconstituted in buffer (10 mM trizma hydrochloride, 1.0 mM magnesium

chloride, pH 7.4) before use. Synthesis and purity were confirmed by the vendor using mass spectrometry. UV absorbance was used to confirm concentration of DNA. Additional chemical information can be found in Supporting Information S1. All other chemicals were reagent grade and were used as received.

- 2.2 Aptamer Selection. DNA aptamers were identified through a modified SELEX protocol, similar to what has been previously described.[13] Details of the selection, PCR, cloning, and sequencing can be found in Supporting Information S1. Briefly, an 80 nucleotide structure was used for the initial DNA library with a 40 nucleotide variable region and 20 nucleotide primer-binding sites on each end. Eight rounds of selection were completed for affinity of aptamer sequences binding to commercially-available HAP. The fourth round of selection was a negative selection against commercially-available amorphous calcium phosphate (ACP). FT-IR spectra, showing differences in crystalline structure, are available for these three materials in Supporting Information S2. Evolutionary pressure was added by systematically decreasing the time allowed for binding from 120 min to 5 min over the eight rounds of selection. After cloning and DNA sequencing, resulting aptamer sequences were aligned and analyzed using Geneious software.[36] Aptamer sequences of interest can be found in Table 1 and in Supporting Information S3 and were synthesized commercially for further analysis.
- 2.3 Circular Dichroism. Aptamer sequences of interest, found in Table 1, were analyzed using an Applied Photophysics C S/2 Chirascan circular dichroism instrument. Aptamers were dissolved to 5 μM concentration in Tris-Mg buffer with 100 mM added NaCl, 100 mM KCl, or 100 mM CaCl₂. All samples were annealed to 95 °C, cooled to room temperature, and stored on ice prior to analysis. Spectra were collected from 340 to 220 nm and the data was smoothed using Origin software.

2.4 Quartz Crystal Microbalance Analysis. Quartz crystal microbalance (QCM) quartz crystals (1 in, 5 MHz, Stanford Research Systems) with Ti/Au polished electrodes were used in all experiments with an SRS Research QCM200 instrument and 100 µL axial flow cell. HAP was adhered to the gold electrode by spin-coating a 1 mg mL⁻¹ sonicated suspension in ethanol, as previously described.[37] Surfaces were reused after rinsing in three washes of 6 M HCl to dissolve the mineral layer, followed by DI water and ethanol rinses, and drying with airflow. A new HAP coating was used for each binding experiment. A peristaltic pump (Master-flex C/L) and Tygon tubing (Cole-Parmer 0.020 in ID 0.092 in OD) was used to delivery Tris-Mg running buffer at a flow rate of 29 µL min⁻¹ and a stable QCM baseline was collected for a minimum of 10 min. DNA aptamer samples were diluted in the running buffer and annealed at 95 °C for 2 min and cooled to 25 °C for 0.5 min in a Bio-Rad T100 Thermal Cycler prior to use. Aptamer dilutions were injected over the QCM-HAP surface for 5.0 min to measure adsorption followed by rinsing with running buffer for a minimum of an additional 10 min. Frequency and resistance measurements were made in real time (1 s⁻¹ data collection) and used together to account for non-rigid density and viscosity effects and to calculate the mass of DNA aptamer adsorbed, as previously described. [29,37,38]

Kinetic information can be calculated from the time-dependent binding curves, seen in Figure 1, through fitting to the exponential (eq 2) and plotting τ^{-1} versus C (eq 3), where m_t is the mass at time (t), m_i is the mass at an infinite time, τ^{-1} is the time constant, k_f is the forward rate constant and k_r is the reverse rate constant.[37,39]

$$\ln\left(1 - \frac{m_t}{m_i}\right) = -\tau^{-1}t\tag{2}$$

$$\tau^{-1} = k_f C + k_r \tag{3}$$

Constants were obtained from regression analysis of the linear plot (eq 3). Error in these values is given as standard deviation propagated from the regression analysis of the linear fit from low concentration without monolayer surface saturation.

A Langmuir Isotherm model was fit to each data set to estimate affinity binding constant, K_a, as previously described,[29,37,38]

$$\frac{C}{Q} = \frac{1}{N}C + \frac{1}{K_Q N} \tag{1}$$

where, C is the initial concentration of DNA aptamer in solution in M, Q is the mass of material bound in g, and K_a is the adsorption affinity constant with units of M^{-1} . Constants were obtained from regression analysis of the linear plot of C/Q against C (Supporting Information S3). Error in these values is given as standard deviation propagated from the regression analysis of the linear fit, where a minimum of six data points were used to calculate each value.

2.5 Competitive Binding Assay. One aptamer sequence (1) was synthesized with a FAM fluorescent tag attached to the 5' end (1F), the end opposite from the G-quadruplex secondary structure (Table 1), and was further studied in a competitive binding assay. All aptamers were annealed before use and combined with HAP suspensions as described above. Experiments were conducted where aptamer (1F) was mixed with aptamer (2) or aptamer (3), each at 250 nM, prior to the addition of the HAP suspension. After 30 min of reaction, the sample was centrifuged at 13,000 RPM for 5 min and 100 μ L of the supernatant was removed and diluted by a factor of 100 in Tris-Mg buffer. Fluorescence measurements were made with excitation at 495 nm and emission at 517 nm using a Horiba Fluoro-Max 4 instrument.

2.6 Aptamer Selectivity. DNA aptamer samples were prepared at 400 nM concentration in Tris-Mg buffer with 0 or 100 mM added NaCl and annealed as described above. HAP nanopowder, NIST standard HAP, ACP, and TCP were tested for binding selectivity. Suspensions of calcium phosphate materials were prepared in Tris-Mg buffer at 5 mg/mL and sonicated for two minutes to disperse the solid. A 0.09 mL portion of the suspension was added to 0.5 mL of the DNA aptamer solution and vortexed to mix. A second sample of DNA aptamer at the same concentration was kept as a control with added buffer in place of the mineral suspension. After 5 min, both samples were centrifuged at 5,600 RPM for 5 min and 100 µL of the supernatant was removed for absorbance measurement at 260 nm using a Molecular Devices Spectro-Max plate reader instrument. Concentrations of DNA aptamer in solution was calculated using known molar absorptivity and percent binding was found for each sample. Selectivity coefficients were calculated as the ratio of binding to HAP over ACP. Fluorescence binding assays were completed as above, but after a 5 min reaction and centrifugation, the calcium phosphate pellet was washed in Tris-Mg buffer three times. A hand-held UV-visible lamp (365 nm) was used to excite the fluorophore and fluorescence emission was recorded with digital photography. Similarly, samples of nano-HAP and ACP were prepared in a 50% ethanol solution and pipetted onto a gold-coated glass slide (Electron Microscopy Sciences) in the shape of an E with nano-HAP and the shape of a C with ACP. Aptamer 1F at 250 nM in Tris-Mg buffer was added to the surface and incubated for 10 min. The solution was carefully removed and replaced with fresh Tris-Mg buffer prior fluorescence excitation and imaging as above.

3. Results and Discussion

DNA aptamers are well known affinity reagents for small molecules, proteins, viruses, and cells, but have not been widely studied as materials binders.[2-4] Here we report DNA aptamer

sequences that bind to calcium phosphate materials identified through the Systematic Evolution of Ligands by Exponential Enrichment (SELEX)[2-4] and report the analysis of one aptamer in comparison to control sequences. The SELEX protocol was designed to isolate DNA aptamers that bind at a fast rate and with selectivity to crystalline HAP, the primary mineral component in mature bone and enamel, over non-crystalline amorphous calcium phosphate (ACP), a known transient precursor to HAP.[34] This selectivity was achieved by reducing the reaction time during each round of selection from 120 min to 5 min and by completing a negative selection against preformed ACP (selection details in Supporting Information, S1). After eight rounds of selection, 59 sequences were identified and analyzed using Geneious software [36] and ordered into six groups. Representative sequences from those groups can be found in Supporting Information, S3. An important finding from the analysis of these sequences is an average %G nucleotide content of 41 + 9 %, which is significantly higher than the 25% expected in a random sequence of DNA. This constitutes a 64% enrichment in G nucleotides and indicates the success of the SELEX protocol in establishing a consensus motif. The average G-score[40] for the 59 sequences was 24 + 17 with 73% of the sequences being capable for forming a G-quadruplex secondary structure. This enrichment in G nucleotides and a possibility of G-quadruplex formation agrees with previous selections involving calcium phosphate and with known interactions between G-quadruplex structures and Ca²⁺ cations.[13,42-44] To further explore the importance of the G-quadruplex structure, one specific aptamer sequence, Aptamer 1, was analyzed in comparison to Aptamer 2, a sequence with the same %G but without the potential for G-quadruplex formation, and Aptamer 3, a sequence with 24% G nucleotides (Table 1). All three aptamers have approximately the same Gibb's Free Energy (ΔG) for internal Watson-Crick base-pairing, [41] but only Aptamer 1 is capable of forming a G-quadruplex. Circular dichroism analysis of these three aptamers in the

Table 1. Sequences, %G, G-score, and Gibb's Free Energy of folding for aptamers

Aptamer	Sequence	%G	$G_s{}^i$	ΔG ⁱⁱ (kcal mol ⁻¹)
1	CAGGGCGCTACGGTATGTGTTG <u>GG</u> TCT <u>GG</u> CGTA <u>GG</u> GCT <u>GG</u> C	46	35	-7.37
1 F	F-CAGGGCGCTACGGTATGTGTTG <u>GG</u> TCT <u>GG</u> CGTA <u>GG</u> GCT <u>GG</u> C	46	35	-7.37
2	GAGCGCGCTACGGTATGTGTTGCGTGTGGCGTAGCGGTGCG	46	0	-8.54
3	CAGCGCCCTACGCTATGTCTTGCGTCTCGCCTAGCGCTCGC	24	0	-7.99

ⁱCalculated with QGRS Mapper[40]

presence of additional sodium, potassium, and calcium, Supporting Information S3, supports the conclusion that only Aptamer 1 forms a G-quadruplex.[45-47] Aptamer 1F is the same sequence as Aptamer 1, but was synthesized with a FAM fluorescent label at the 5' end, opposite the G-quadruplex structure.

A quartz crystal microbalance (QCM)[29,37,39] instrument was used to analyze adsorption of DNA aptamers to HAP-coated QCM electrodes. Spin-coating was used to present a uniform and rigid layer of HAP material on the QCM surface while maintaining the material in a crystalline phase, as has been previously reported.[37] DNA aptamers were introduced to the HAP-QCM surface with flow in 10 mM Tris-Mg buffer at pH 7.4 and mass adsorption, indicating affinity to HAP, was measured in real time. From mass adsorption plots (Figure 1A), it is apparent that Aptamer 1 binds with a faster rate of adsorption compared to Aptamers 2 and 3. Kinetic analysis (Figure 1B) shows a significantly higher forward rate constant, k_f , for Aptamer 1. This enhancement in rate of adsorption is expected by design of the selection method where reaction

ⁱⁱCalculated with Mfold,[41] 25 °C, 50 mM Na⁺

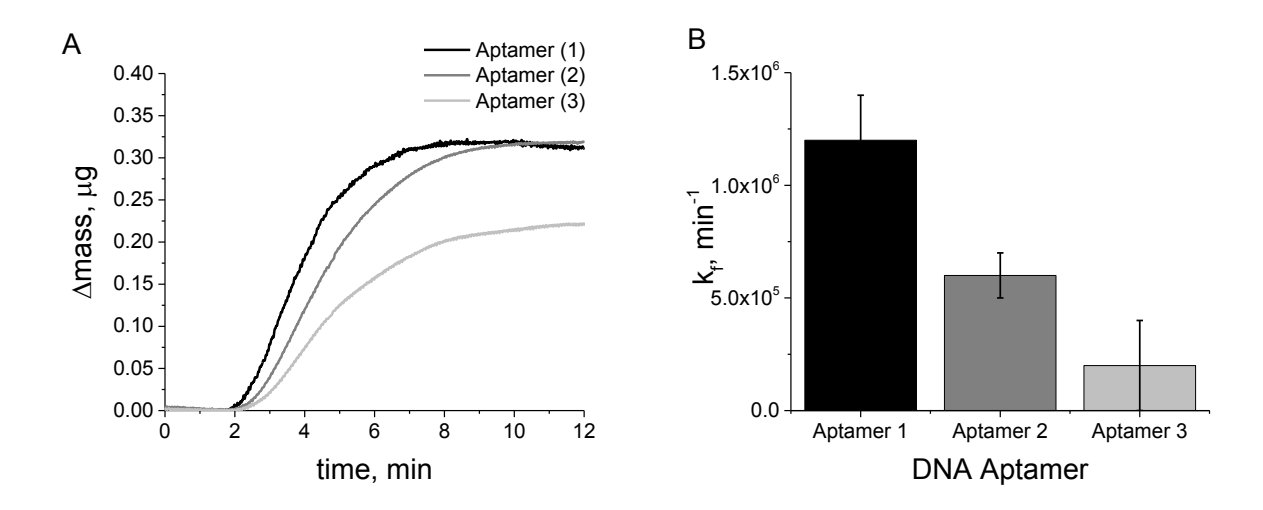


Figure 1. Adsorption binding of DNA aptamers to hydroxyapatite (HAP) measured by quartz crystal microbalance (QCM). **A)** Representative real-time QCM data for three different DNA aptamers all at 400 nM [aptamer]. Differences in binding kinetics and level of saturation are observed. **B)** Kinetic rate constants (k_f) for three different aptamers showing statistically significant differences in adsorption rate constants. P < 0.001 for Aptamer 1 compared to Aptamer 2 and Aptamer 3.

time decreased with each round of selection. We hypothesize that this could be due to a more compact structure for Aptamer 1, possibly due to the G-quadruplex, which would allow a higher diffusion constant and faster binding kinetics.[48]

Fitting a Langmuir isotherm model to data collected at a range of aptamer concentrations allows for the calculation of equilibrium binding information (Table 2 and Supporting Information, S4). Large K_a values and binding at concentrations as low as 50 nM indicate strong affinity for all three aptamers to HAP. It is interesting to note that there are only weak statistical differences in affinity when comparing Aptamer 1 to Aptamers 2 and 3 (K_a, Table 2) The lack of difference in affinity for these aptamers is somewhat surprising, but not completely unexpected due to the molecular nature of DNA and the selection method. DNA is a negatively charged poly-anion that is stabilized by positive charge, such as the Ca²⁺ in HAP, suggesting that all DNA sequences will have some affinity for the HAP mineral. This has been previously demonstrated in HAP chromatography and

in the use of HAP to deliver DNA intracellularly.[49-51] The SELEX method used here did not bias the selection towards affinity, but rather towards enhanced kinetic binding, which has been demonstrated (Figure 1). It is also possible that K_a values could change as secondary structure changes with increasing ionic strength. It has been previously demonstrated[13,28] that aptamer sequences with G-quadruplex structures have a higher affinity to HAP, relative to other sequences,

Table 2. Aptamer affinity and kinetics for binding to HAP.

Aptamer	k _f , min ⁻¹	$K_a, M^{\text{-}1}$	N, mol m ⁻²	Footprint, nm ² aptamer ⁻¹
1	$12 \pm 2 \times 10^5$	$3.0 \pm 0.9 \times 10^6$	$6.1 \pm 0.1 \times 10^{-7}$	2.7 ± 0.5
2	$6 \pm 1 \times 10^5$	$7 \pm 4 \times 10^6$	$4.1 \pm 0.5 \times 10^{-7}$	4.1 ± 0.5
3	$2 \pm 2 \times 10^5$	$7 \pm 4 \times 10^6$	$3.2 \pm 0.4 \times 10^{-7}$	5.1 <u>+</u> 0.6

when increased ionic strength is used to stabilize the G-quadruplex. Binding capacity in mol m⁻² or footprint in nm² aptamer⁻¹ (Table 2) shows a statistically significant difference between aptamers with Aptamer 1 having a higher loading capacity or smaller footprint per aptamer. This is expected since Aptamer 1 could form a G-quadruplex with a more compact secondary structure as opposed to Aptamers 2 or 3 with potentially extended conformations and agrees with the enhanced kinetic binding and potentially higher diffusion constant discussed above.

The differences in kinetics of binding were further explored using a competitive assay. It was expected that in a competitive format, Aptamer 1 would show the greatest binding due to a larger k_f despite the finding that equilibrium constants, K_a , are nearly identical. Fluorescently-labeled

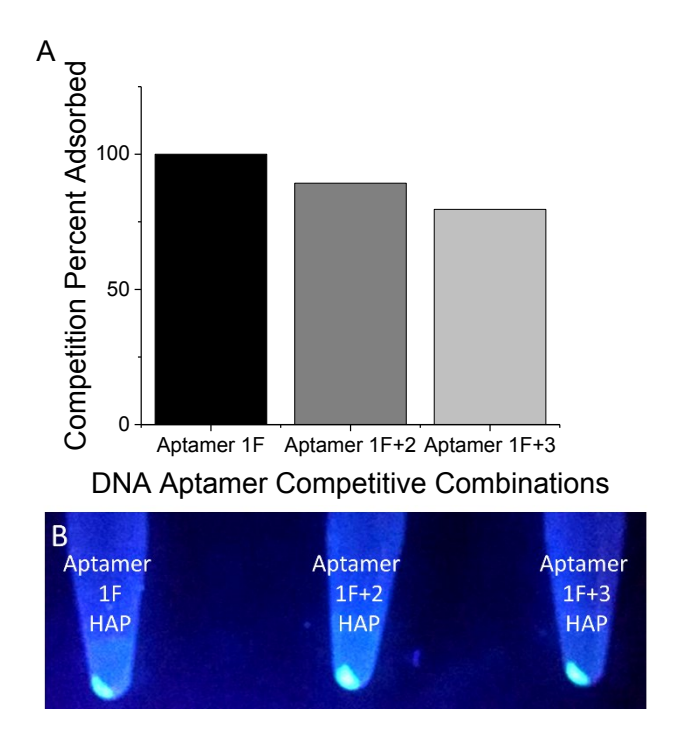


Figure 2. Competitive binding of Aptamer 1F in the presence of Aptamer 2 or Aptamer 3 at 250 nM concentration. **A)** Percent adsorption shows the percent of Aptamer 1F adsorbed to nano-HAP in the absence of any competitor or in the presence of other DNA aptamer strands measured by solution fluorescence spectroscopy. **B)** Fluorescence of Aptamer 1F binding to nano-HAP in the absence of any competitor or in the presence of other DNA aptamer strands.

Aptamer 1F was pre-mixed with Aptamer 2 and with Aptamer 3 in separate experiments, then added to a suspension of HAP. The amount of Aptamer 1F remaining in solution or the amount found on the surface of the HAP was measured to indicate the extent of binding. If the amount of binding to HAP when comparing Aptamer 1F and Aptamer 2 or Aptamer 3 were equal, we would expect 50% binding for Aptamer 1F. As seen in Figure 2A, Aptamer 1F out-competed both Aptamer 2 and Aptamer 3 with 89% and 79% binding, respectively. This indicates that Aptamer 1F was able to adsorb with faster kinetics and stayed adsorbed to HAP in the presence of Aptamer 2 or Aptamer 3. A visual representation of this can be found in Figure 2B where strong fluorescence was observed on the mineral pellet in all three cases, indicating that Aptamer 1F bound competitively in all cases.

Aptamers were found to have exceptional selectivity to HAP over two other calcium phosphates, ACP and TCP (β-tricalcium phosphate), as seen in Figure 3 and Supporting Information S5. ACP and TCP were studied in comparison to HAP because they have similar ionic formulas to HAP, all being calcium phosphates, but with different crystallinities. Selectivity was determined by combining DNA aptamers with specific mass amounts of calcium phosphate materials with different crystallinities and either measuring the absorbance of aptamer remaining in solution or by measuring the fluorescence of Aptamer 1F on the mineral pellet. Selectivity coefficients were calculated as the ratio of average percent binding to HAP to average percent binding to ACP. Adsorption was significantly greater for all aptamers binding to both nano-HAP and the NIST standard HAP compared to ACP and TCP as seen in Figure 3A. In lower ionic strength solution conditions, Tris-Mg buffer with no added NaCl, selectivity coefficients ranged from 3 to 8 with Aptamer 3 showing a slightly higher selectivity. When ionic strength was increased by adding 100 mM NaCl, the selectivity coefficients ranged from 19 to 108, with Aptamer 1 showing the highest selectivity. We hypothesize that the increase in ionic strength increases the stability of the Gquadruplex in Aptamer 1 and decreases weaker affinity adsorption possibly seen in Aptamers 2 and 3. These results indicate that adsorption is not solely based on electrostatic interactions between the anionic DNA aptamer and the Ca²⁺ in the mineral, since HAP, ACP, and TCP are all calcium phosphate materials. It may be that there are preferential binding sites on the crystalline HAP where DNA more readily binds or binds with a greater capacity compared to amorphous or non-HAP material. Computational studies by del Valle, et al.[52] support this hypothesis by suggesting that particular crystal faces of HAP are favorable for DNA double helix adsorption.

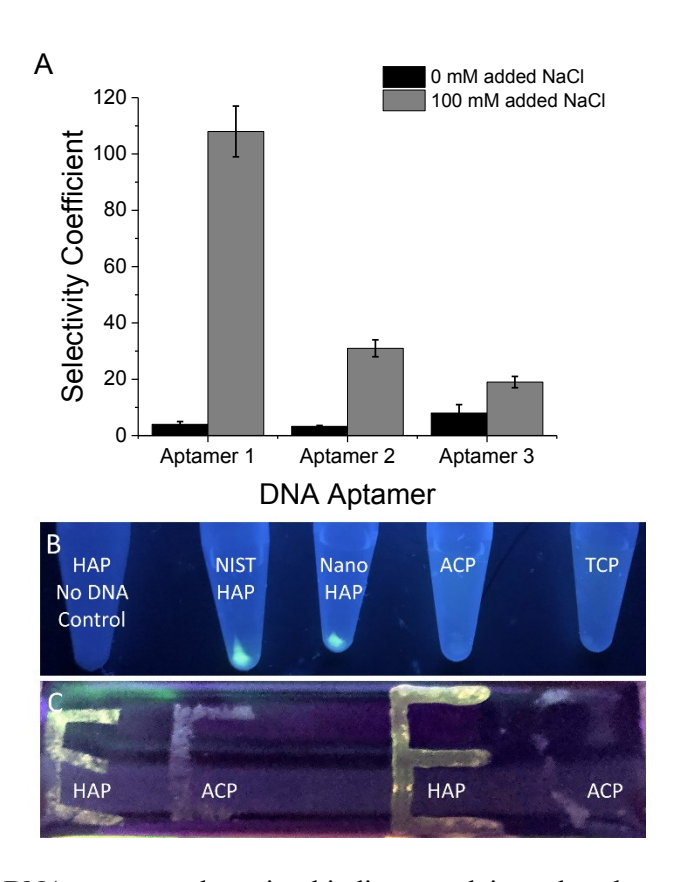


Figure 3. Selectivity of DNA aptamer adsorption binding to calcium phosphate materials. **A)** Selectivity coefficient for aptamer adsorption comparing HAP to ACP materials at lower and higher ionic strength solution conditions. **B)** Fluorescence of Aptamer **1F** shows specific binding to NIST and nano-HAP over amorphous calcium phosphate (ACP) and tricalcium phosphate (TCP). **C)** Fluorescence of Aptamer **1F** shows specific binding to surface deposited nano-HAP over ACP in duplicate experiments.

This may theoretically apply to G-quadruplex structures as well and these crystalline faces may be inaccessible in amorphous material.

The increased selectivity of Aptamer 1 is also expected due to the negative selection used in round 4 of the SELEX procedure. This selectivity is apparent in Figure 3B where Aptamer 1F clearly binds selectively to HAP materials over ACP and TCP. Selectivity was further tested in a surface labeling format where HAP and ACP were deposited on a gold-coated surface through physisorption then labeled with Aptamer 1F. Mineral was deposited in the shape of the letters EC, for Emmanuel College, with nano-HAP used for the E and ACP used for the C, seen in Figure 3C.

The HAP material showed a 2.5 ± 0.5 times intensity increase for a similar area of mineral over the ACP material in fluorescence imaging and Image J analysis. This indicates that Aptamer **1F** could be employed in microscopy studies where there is a need to label HAP, but not amorphous material. Currently available fluorescent reagents for calcium phosphate materials tend to fluorescence in the presence of any calcium cation and do not distinguish between crystallinity or morphology.[33]

4. Conclusions

These results have highlighted the successful selection of a DNA aptamer with interesting and useful attributes for an affinity reagent for calcium phosphate materials. Aptamer 1, for example, has a high selectivity to crystalline HAP over non-HAP calcium phosphates, binds with fast kinetics, 1.2 x 10⁶ min⁻¹, and preferentially binds to HAP in competitive binding experiments over other aptamer sequences. Equilibrium binding constants were similar for all aptamers tested, with Aptamer 1 having a K_a of $3.0 \pm 0.9 \times 10^6 \, M^{-1}$, demonstrating high affinity. This aptamer could be compared to short peptide sequences identified through phage-display technology, [53,54] though these previous studies did not report affinity constants or selectivity towards different phases of mineral. Phage-display work instead focused on the potential for the peptide to control calcium phosphate mineralization, which we have already reported for different DNA aptamer sequences.[13,28] We anticipate that fluorescently-labeled or gold nanoparticle-labeled aptamers would have potential as affinity and labeling reagents in light microscopy or electron microscopy where differentiation between crystalline and amorphous material would be beneficial. For example, the analysis of transient amorphous mineral observed in enamel and bone formation [34] is currently analyzed primarily through spectroscopy such as energy dispersive spectroscopy (EDS), x-ray photoelectron spectroscopy (XPS), or even using synchrotron sources, all of which

require additional and specific sample preparation.[55] The identification procedures for calcified arterial plaques[35] or micro-calcifications related to breast cancer[56] may benefit from a biochemistry-friendly affinity reagent. Given the programmability and synthetic ease associated with DNA aptamers, it is also possible to envision enhanced sensitivity gained through PCR amplification strategies where only small amounts of calcium phosphate materials are available. These examples point to exceptional future utility in biomedical and biotechnology fields where the labeling and imaging of biomaterials is required.

Supporting Information

The following is available as supporting information: Complete SELEX protocol and methods, aptamer sequences from selection, circular dichroism spectra, adsorption binding curves and Langmuir isotherm plots, binding selectivity data.

Funding Sources

This work was funded by Emmanuel College and the National Science Foundation, Division of Materials Research (1306117).

Acknowledgements

The authors would like to thank Samantha Watson, Alexander Paige, and Padraig Deighan of Emmanuel College for their guidance and discussion. The authors would like to thank the Boston University Chemical Instrumentation Center for access to and assistance with circular dichroism spectroscopy.

References

Reference List

- [1] A.D. Keefe, S. Pai, A. Ellington, Aptamers as therapeutics, Nature Rev. Drug Disc. 9 (2010) 537-550.
- [2] Y.X. Wu, Y.J. Kwon, Aptamers: The "evolution" of SELEX, Methods. (2016).
- [3] T.A. Feagin, N. Maganzini, H.T. Soh, Strategies for Creating Structure-Switching Aptamers, ACS Sens. 3 (2018) 1611-1615.
- [4] M. Yuce, N. Ullah, H. Budak, Trends in aptamer selection methods and applications, Analyst. 140 (2015) 5379.
- [5] A. Csordas, A.E. Gerdon, J.D. Adams, J. Qian, S.S. Oh, Y. Xiao, H.T. Soh, Detection of Proteins in Serum by Micromagnetic Aptamer PCR (MAP) Technology, Angew. Chem. Int. Ed. 122 (2010) 365-368.
- [6] S. Meyer, J.P. Maufort, J. Nie, R. Stewart, B.E. McIntosh, L.R. Conti, K.M. Ahmad, H.T. Soh, J.A. Thomson, Development of an Efficient Targeted Cell-SELEX Procedure for DNA Aptamer Reagents, PLoS One. 8 (2013) e71798.
- [7] D. Sun, J. Lu, L. Zhang, Z. Chen, Aptamer-based electrochemical cytosensors for tumor cell detection in cancer diagnosis: A review, Analytica Chimica Acta. 1082 (2019) 1-17.
- [8] X. Pang, C. Cui, S. Wan, Y. Jiang, L. Zhang, L. Xia, L. Li, X. Li, W. Tan, Bioapplications of Cell-SELEX-Generated Aptamers in Cancer Diagnostics, Therapeutics, Theranostics and Biomarker Discovery: A Comprehensive Review, Cancers. 10 (2018) 47.
- [9] H. Sun, W. Tan, Y. Zu, Aptamers: versatile molecular recognition probes for cancer detection, Analyst. 141 (2016) 403.
- [10] K. Sefah, J.A. Phillips, X. Xiong, L. Meng, D. Van Simaeys, H. Chen, J. Martin, W. Tan, Nucleic acid aptamers for biosensors and bio-analytical applications, Analyst. 134 (2009) 1765-1775.
- [11] F. Li, Z. Yu, X. Han, R.Y. Lai, Electrochemical aptamer-based sensor for food and water analysis: A review, Analytica Chimica Acta. 1051 (2019) 1-23.
- [12] L.A. Bawazer, A.M. Newman, Q. Gu, A. Ibish, M. Arcila, J.B. Cooper, F.C. Meldrum, D.E. Morse, Efficient Selection of Biomineralizing DNA Aptamer Using Deep Sequencing and Population Clustering, ACS Nano. 8 (2014) 387-395.

- [13] K.R. Baillargeon, K. Meserve, S. Faulkner, S. Watson, H. Butts, P. Deighan, A.E. Gerdon, Precipitation SELEX: identification of DNA aptamers for calcium phosphate materials synthesis, Chem. Commun. 53 (2017) 1092.
- [14] X. Liu, F. Zhang, X. Jing, M. Pan, P. Liu, W. Li, B. Zhu, J. Li, H. Chen, L. Wang, J. Lin, Y. Liu, D. Zhao, H. Yan, C. Fan, Complex silica composite nanomaterials templated with DNA origami, Nature. 559 (2018) 593.
- [15] P.A. Mirau, J.E. Smith, J.L. Chavez, J.A. Hagen, N. Kelley-Loughnane, R. Naik, Structured DNA Aptamer Interactions with Gold Nanoparticles, Langmuir. 34 (2018) 2139-2146.
- [16] L. Wang, Z. Zhang, B. Liu, Y. Liu, A. Lopez, J. Wu, J. Liu, Interfacing DNA Oligonucleotides with Calcium Phosphate and Other Metal Phosphates, Langmuir. 34 (2018) 14975-14982.
- [17] L. Ma, B. Liu, P.-.J. Huang, X. Zhang, J. Liu, DNA Adsorption by ZnO Nanoparticles near Its Solubility Limit: Implications for DNA Fluorescence Quenching and DNAzyme Activity Assays, Langmuir. 32 (2016) 5672-5680.
- [18] C. Lu, Z. Huang, B. Liu, Y. Liu, Y. Ying, J. Liu, Poly-cytosine DNA as a High-Affinity Ligand for Inorganic Nanomaterials, Angew. Chem. Int. Ed. 56 (2017) 6208-6212.
- [19] B. Liu, J. Liu, Comprehensive Screen of Metal Oxide Nanoparticles for DNA Adsorption, Fluorescence Quenching, and Anion Discrimination, ACS Appl. Mater. Interfaces. 7 (2015) 24833-24838.
- [20] Y. Zhou, Z. Huang, R. Yang, J. Liu, Selection and Screening of DNA Aptamers for Inorganic Nanomaterials, Chem. Eur. J. 24 (2018) 2525-2532.
- [21] Y. Wang, N.S.R. Satyavolu, Y. Lu, Sequence-specific control of inorganic nanomaterials morphologies by biomolecules, Curr. Opin. Coll. Interface Sci. 38 (2018) 158-169.
- [22] S.Y. Kwak, A. Litman, H.C. Margolis, Y. Yamakoshi, J.P. Simmer, Biomimetic Enamel Regeneration Mediated by Leucine-Rich Amelogenin Peptide, J. Dent. Res. 96 (2017) 524-530.
- [23] K. Mukherjee, Q. Ruan, S. Nutt, J. Tao, J.J. De Yoreo, J. Moradian-Oldak, Peptide-Based Bioinspired Approach to Regrowing Multilayered Aprismatic Enamel, ACS Omega. 3 (2018) 2546-2557.
- [24] B. Wingender, P. Bradley, N. Saxena, J.W. Ruberti, L. Gower, Biomimetic organization of collagen matrices to template bone-like microstructures, Matrix Biol. 52-54 (2016) 384-396.
- [25] A.K. Burwell, T. Thula-Mata, L.B. Gower, S. Habeliz, M. Kurylo, S.P. Ho, Y. Chien, J. Cheng, N.F. Cheng, S.A. Gansky, S.J. Marshall, G.W. Marshall, Functional Remineralization of Dentin Lesions Using Polymer-Induced Liquid-Precursor Process, PLoS One. 7 (2012) e38852.

- [26] L.C. Palmer, C.J. Newcomb, S.R. Kaltz, E.D. Spoerke, S.I. Stupp, Biomimetic Systems for Hydroxyapatite Mineralization Inspired by Bone and Enamel, Chem. Rev. 108 (2008) 4754-4783.
- [27] A.J. Lausch, B.D. Quan, J.W. Miklas, E.D. Sone, Extracellular Matrix Control of Collagen Mineralization In Vitro, Adv. Funct. Mater. 23 (2013) 4906-4912.
- [28] J. Shlaferman, A. Paige, K. Meserve, J.A. Miech, A.E. Gerdon, Selected DNA Aptamers Influence Kinetics and Morphology in Calcium Phosphate Mineralization, ACS Biomater. Sci. Eng. 5 (2019) 3228-3236.
- [29] S.C. Ngourn, H.A. Butts, A.R. Petty, J.E. Anderson, A.E. Gerdon, Quartz Crystal Microbalance Analysis of DNA-Templated Calcium Phosphate Mineralization, Langmuir. 28 (2012) 12151-12158.
- [30] G. Revilla-Lopez, J. Casanovas, O. Bertran, P. Turon, J. Puiggali, C. Aleman, Modeling biominerals formed by apatites and DNA, Biointerphases. 8 (2013) 10.
- [31] G. Revilla-Lopez, A.M. Rodriguez-Rivero, L.J. del Valle, J. Puiggali, P. Turon, C. Aleman, Biominerals Formed by DNA and Calcium Oxalate or Hydroxyapatite: A Comparative Study, Langmuir. 35 (2019) 11912-11922.
- [32] F. Kim, T. Chen, T. Burgess, P. Rasie, T.L. Selinger, A. Greschner, G. Rizis, K. Carneiro, Functionalized DNA nanostructures as scaffolds for guided mineralization, Chem. Sci. 10 (2019) 10537-10542.
- [33] J.T. Russell, Imaging calcium signals in vivo: a powerful tool in physiology and pharmacology, Brit. J. of Pharmacol. 163 (2011) 1605-1625.
- [34] E. Beniash, R.A. Metzler, R.S.K. Lam, P.U.P.A. Gilbert, Transient amorphous calcium phosphate in forming enamel, J. Struct. Biol. 166 (2009) 133-143.
- [35] R. Coscas, M. Bensussan, M. Jacob, L. Louedec, Z. Massy, J. Sadoine, M. Daudon, C. Chaussain, D. Bazin, J. Michel, Free DNA precipitates calcium phosphate apatite crystals in the arterial wall in vivo, Atherosclerosis. 259 (2017) 60-67.
- [36] M. Kearse, R. Moir, A. Wilson, S. Stones-Havas, M. Cheung, S. Sturrock, S. Buxton, A. Cooper, S. Markowitz, C. Duran, T. Thierer, B. Ashton, P. Meintjes, A. Drummond, Geneious Basic: An integrated and extendable desktop software platform for the organization and anlysis of sequence data, Bioinformatics. 28 (2012) 1647-1649.
- [37] C. Connelly, T. Cicuto, J. Leavitt, A. Petty, A. Litman, H.C. Margolis, A.E. Gerdon, Dynamic interactions of amelogenin with hydroxyapatite surfaces are dependent on protein phosphorylation and solution pH, Coll. Surf. B. 148 (2016) 377-384.

- [38] A.E. Gerdon, D.W. Wright, D.E. Cliffel, Quartz Crystal Microbalance Detection of Glutathione-Protected Nanoclusters Using Antibody Recognition, Anal. Chem. 77 (2005) 304-310.
- [39] A.E. Gerdon, D.W. Wright, D.E. Cliffel, Quartz Crystal Microbalance Characterization of Nanostructure Assemblies in Biosensing, in: C. Kumar (Ed.), Characterization Tools for Nanosystems in Life Sciences, 1st ed., Wiley-VCH, New York, 2005, pp. 109-144.
- [40] O. Kikin, L. D'Antonio, P.S. Bagga, QGRS Mapper: a web-based server for predicting G-quadruplexes in nucleotide sequences, Nucl. Acids. Res. 34 (2006) W676-W682.
- [41] M. Zuker, Mfold web server for nucleic acid folding and hybridization prediction, Nucl. Acids. Res. 31 (2003) 3406-3415.
- [42] D. Bhattacharyya, G.M. Arachchilage, S. Basu, Metal Cations in G-Quadruplex Folding and Stability, Front. Chem. 4 (2016) 38.
- [43] M.P.H. Lee, G.N. Parkinson, P. Hazel, S. Neidle, Observation of the coexistence of sodium and calcium ions in a DNA G-quadruplex ion channel, J. Am. Chem. Soc. 129 (2007) 10106-10107.
- [44] D. Miyoshi, A. Nakao, N. Sugimoto, Structural transition from antiparallel to parallel G-quadruplex of d(G4T4G4) induced by Ca2+, Nucl. Acids. Res. 31 (2003) 1156-1163.
- [45] G.T. Hwang, Y. Hari, F.E. Romesberg, The effects of unnatural base pairs and mispairs on DNA duplex stability and solvation, Nucl. Acids. Res. 37 (2009) 4757-4763.
- [46] K. Tsukakoshi, Y. Ikuta, K. Abe, W. Yoshida, K. Iida, Y. Ma, K. Nagasawa, K. Sode, K. Ikebukuro, Structural regulation by a G-quadruplex ligand increases binding abilities of G-quadruplex-forming aptamers, Chem. Commun. 52 (2016) 12646.
- [47] R. del Villar-Guerra, J.O. Trent, J.B. Chaires, G-quadruplex secondary structure from circular dichroism spectroscopy, Angew. Chem. Int. Ed Engl. 57 (2018) 7171-7175.
- [48] M. Kang, C.A. Day, E. DiBenedetto, A.K. Kenworthy, A Quantitative Approach to Analyze Binding Diffusion Kinetics by Confocal FRAP, Biophys. J. 99 (2010) 2737-2747.
- [49] M. Okazaki, Y. Yoshida, S. Yamaguchi, M. Kaneno, J.C. Elliott, Affinity binding phenomena of DNA onto apatite crystals, Biomaterials. 22 (2001) 2459-2464.
- [50] C. Andrews-Pfannkoch, D.W. Fadrosh, J. Thorpe, S.J. Williamson, Hydroxyapatite-Mediated Separation of Double-Stranded DNA, Single-Stranded DNA, and RNA Genomes from Natural Viral Assemblages, Appl. Envron. Microbio. 76 (2010) 5039-5045.

- [51] M.A. Ashaie, R.A. Islam, N.I. Kamaruzman, N. Ibnat, K.K. Tha, E.H. Chowdhury, Targeting Cell Adhesion Molecules via Carbonate Apatite-Mediated Delivery of Specific siRNAs to Breast Cancer Cells In Vitro and In Vivo, Pharmaceutics. 11 (2019) 309.
- [52] L.J. del Valle, O. Bertran, G. Chaves, G. Revilla-Lopez, M. Rivas, M.T. Casas, J. Casanovas, P. Turon, J. Puiggali, C. Aleman, DNA adsorbed on hydroxyapatite surfaces, J. Mater. Chem. B. 2 (2014) 6953.
- [53] J. Mao, X. Shi, Y. Wu, S. Gong, Identification of Specific Hydroxyapatite {001} Binding Heptapeptide by Phage Display and Its Nucleation Effect, Materials. 9 (2016) 700.
- [54] M. Gungormus, H. Fong, I.W. Kim, J.S. Evans, C. Tamerler, M. Sarikaya, Regulation of in vitro Calcium Phosphate Mineralization by Combinatorially Selected Hydroxyapatite-Binding Peptides, Biomacromolecules. 9 (2008) 966-973.
- [55] E. DiMasi, L.B. Gower, Biomineralization Sourcebook: Characterization of Biominerals and Biomimetic Materials, (2014) 432.
- [56] S. Choi, S. Coonrod, L. Estroff, C. Fischbach, Chemical and physical properties of carbonated hydroxyapatite affect breast cancer cell behavior, Acta Biomater. 24 (2015) 333-342.